Ultrafast Excitation Energy Transfer in Small Semiconducting Carbon Nanotube Aggregates

Larry Lüer,[†,‡,*] Jared Crochet,[§,⊥] Tobias Hertel,[¶] Giulio Cerullo,[#] and Guglielmo Lanzani[▽]

[†]Madrid Institute of Advanced Studies (IMDEA Nanociencia), Madrid, Spain, [‡]CNR/INFM-ULTRAS, Politecnico di Milano, Italy, [§]Institut für Physikalische und Theoretische Chemie, Universität Würzburg, Germany, and [⊥]Center for Integrated Nanotechnologies, Los Alamos National Laboratory, New Mexico, 87545, [¶]Institut für Physikalische und Theoretische Chemie, Universität Würzburg, Germany, [#]Dipartimento di Fisica, Politecnico di Milano, Milan, Italy, [▽]Center for Nanoscience and Technology of IIT @ POLIMI and Physics Department of Politecnico di Milano, Milan, Italy

ABSTRACT We study excitation energy transfer in small aggregates of chirality enriched carbon nanotubes by transient absorption spectroscopy. Ground state photobleaching is used to monitor exciton population dynamics with sub-10 fs time resolution. Upon resonant excitation of the first exciton transition in (6,5) tubes, we find evidence for energy transfer to (7,5) tubes within our time resolution (<10 fs). Excitation in the visible spectral range, where the second excitonic transitions occur, is followed by fast intratube relaxation and subsequent energy transfer, in particular from the (8,4) tube toward other tubes, the latter process occurring in less than 10 fs.

KEYWORDS: carbon nanotubes · femtosecond spectroscopy · excitation energy transfer · optoelectronics · aggregates · chirality enrichment · excitons

Carbon nanotubes (CNTs) are promising candidates for nanotechnology-based optoelectronics owing to outstanding physical properties including well-defined optical resonances, ultrafast nonlinear responses, and ballistic 1D charge transport.[1] The ground state electronic structure can be described by delocalized π-electrons confined to a rolled-up, high aspect ratio graphene sheet that results in *quasi*-1D electronic states. Low energy optical transitions are associated with the formation of Coulomb correlated electron−hole pairs that are often described as 1D Wannier−Mott excitons.[2] These excitons have been found to be a few nanometers in size[3] and give rise to intriguing optical properties that have stimulated both fundamental and applied research efforts.[4−7] In response to the technological difficulties of fabricating single nanotube electro-optic devices, solid state networks of CNTs, containing a broad distribution of aggregated tubes with different diameters and chiralities, have emerged as exceptional materials with tunable electronic properties.[8] To realize the full potential of CNT networks it is essential to obtain a better understanding of their photophysics and excitation dynamics. In spite of their complex electronic structure, the interpretation of CNT optical properties has so far been based on intratube properties, while intertube interactions have been largely neglected. Intertube coupling however should play an important role in such systems given the crystalline structure of nanotube aggregates. Only recently has energy transfer (ET) been addressed by photoluminescence (PL) excitation spectroscopy.[9−13] Such studies probe the steady state population of emissive states and ET is difficult to distinguish from defect induced emission satellites.[14] Unambiguous spectroscopic signatures of ET have been demonstrated in air-suspended binary aggregates.[15] While fluorescence spectroscopy is well suited to obtain ET transfer yields, it is usually difficult to derive the ET transfer rate, k_{ET}, in ensembles, because the aggregation effect on the nonradiative decay kinetics cannot *a priori* be known. Generally, fluorescence spectroscopy preferentially probes isolated nanotubes, while emission from aggregated tubes is more likely overlooked due to PL quenching. So far ET in pairs of carbon nanotubes, deposited on substrates, showed a strongly distance-dependent transfer rate in tip-enhanced luminescence studies. The strong distance dependence points to a resonance type transfer mechanism,[16] with a lower limit of $k_{ET} > 5 \times 10^{11}$ s^{-1}. This value has been obtained from the ET *yields*, measured directly, taking into consideration the tip-induced enhancement of radiative and nonradiative rate constants. It can be concluded that ET in a pseudohexagonal crystal, composed of CNTs at van der Waals distance, proceeds at an even higher rate, outpacing any kind of competing process.

*Address correspondence to larry.luer@imdea.org.

Received for review April 2, 2010 and accepted May 27, 2010.

Published online June 2, 2010.
10.1021/nn100674h

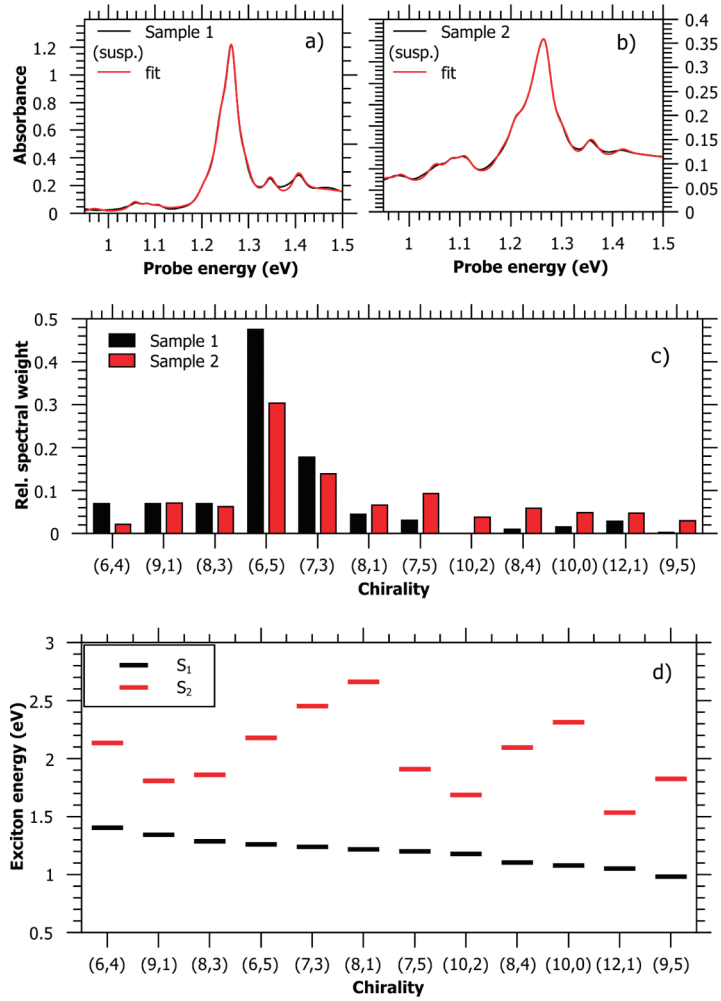

Figure 1. Ground state absorption spectra (black curves) of the suspensions from which sample 1 (a) and sample 2 (b) were obtained and multi-Voigt band fits (red curves), after subtraction of a broad absorption background. (c) Relative spectral weight for the most abundant chiralities, as results from the *multi*-Voigt band fits in panels a and b. (d) S_2 and S_1 energies, respectively, according to literature data.[36]

In this work, we study the ET in small aggregates of CNTs of different chiralities in the time domain, with unprecedented time resolution, by using femtosecond transient absorption spectroscopy with broadband few-optical-cycle pulses, providing a temporal resolution down to 10 fs. The transient photobleaching of excitonic features indicates that ET rates are ultrafast, exceeding 10^{14} s^{-1}.

RESULTS AND DISCUSSION

In the following study, we compare two CNT samples, containing, respectively, a low (sample 1) and high (sample 2) percentage of aggregates. Intertube effects, like ET, should therefore be enhanced in sample 2 (details of sample preparation are given in the Methods section). Figure 1a (b) shows the ground state absorption spectrum of the suspension from which sample 1 (2) has been obtained.[17] Both panels show a series of maxima which are due to $S_0 \rightarrow S_1$ transitions in tubes of various chiralities.[18] A multi-Voigt line shape analysis (dashed lines in Figure 1a,b) gives the spectral weights of different tube types found in the histogram of Figure 1c. Note, that a tube's spectral weight is proportional to the product of tube concentration and oscillator strength. Oscillator strengths depend on tube chirality, diameter, and possibly doping[19] and therefore need to be accounted for if spectral weights from tubes with widely different structural properties are to be compared. However, tubes within the narrow diameter range used in this study are expected to have similar oscillator strengths, and we therefore tentatively associate concentration with spectral weight.

Figure 1c clearly shows that the procedure used for isolation and chirality enrichment in sample 1 leads to an enhancement of small (and thus high optical bandgap, see Figure 1d) CNTs and to a strong suppression of larger CNT with smaller optical bandgaps. The most prominent CNT in both cases is the (6,5) CNT with a relative abundance of 47% (30%) for sample 1 (2).

In Figure 2, we show $\Delta T/T$ spectra at a delay time of $t = 50$ fs between pump and probe pulses for sample 1 and 2 (panel a and b, respectively). For comparison, we include the ground state absorption (GA) spectra of

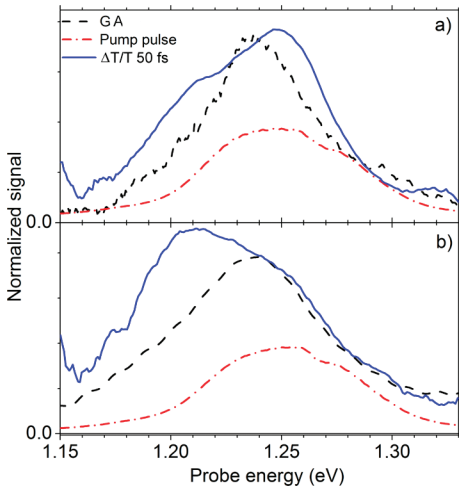

Figure 2. Comparison of $\Delta T/T$ spectrum at 50 fs delay time (blue solid line), ground state absorption (GA, black dashed line), and pump pulse spectrum (red dash−dotted line) for sample 1 (panel a) and sample 2 (panel b).

the respective films and the pump pulse spectrum (dashed and dash-dotted lines, respectively). In panel a, the $\Delta T/T$ spectrum shows a positive band at 1.25 eV with a shoulder at 1.21 eV. In panel b, the main maximum is at 1.21 eV, with a shoulder at 1.25 eV. The positive bands at 1.21 and 1.25 eV can be associated with photobleaching (PB) of the $S_0 \rightarrow S_1$ transitions in (7,5) and (6,5) tubes, respectively.

Figure 3 shows a series of $\Delta T/T$ spectra from $t = -40$ fs to $t = +50$ fs for both samples 1 and 2 (panel a and b, respectively). We see for both samples that the PB at 1.21 eV shows a delayed build-up with respect to the PB at 1.25 eV. While the PB band at 1.25 eV reaches its maximum at $t = 30$ fs, the PB band at 1.21 eV continues to rise until $t = 50$ fs.

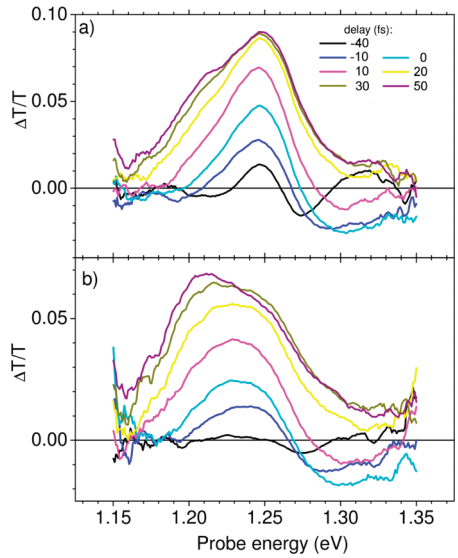

Figure 3. $\Delta T/T$ spectra during and a short time after pumping with 15 fs pulses: (a) sample 1 containing a low amount of aggregates; (b) sample 2 containing a higher amount of aggregates. The pump spectra are given in Figure 2.

Considering the available S_1 energies in Figure 1c, we expect also small contributions from the (8,1) and (7,3) tubes to the PB at 1.25 eV in Figure 2. Note also that in a previous publication, a photoinduced absorption (PA) band at 1.28 eV was reported.[20] This PA band however does not significantly contribute to our spectra on the very fast time scale ($t < 50$ fs) in which we are interested. As Figures 2 and 3 show, there is no sign of such a PA band at 1.28 eV for $t > 10$ fs.[21]

PB is an unspecific probe for the presence of photoexcited states. Apart from neutral excitons, also charge transfer (CT) excitons ("indirect excitons")[22] and separated charge carriers[23] (by virtue of oxidizing/reducing of the respective CNT bands) can give rise to PB of the $S_0 \rightarrow S_1$ transitions. We can exclude CT excitons because these are expected to occur at lower transition energies than direct excitons. In Figure 2, we find that the PB bands occur at the same energy as the respective ground state transitions. We can also exclude separated charge carriers: the intrinsic formation of separated charge carriers requires additional energy in order to overcome the exciton binding energy; however, under our experimental conditions (resonant excitation), this additional energy is not provided. Extrinsic formation of separated charge carriers provides the additional energy, e.g., by the deep trapping of one carrier species, releasing the other; however, carrier trapping does not take place significantly on a 20 fs time scale. In summary, we can exclude any significant contribution from charged photoexcitations and assign the PB bands at 1.21 and 1.25 eV to the presence of S_1 excitons on the respective chiralities. The pump pulse spectrum, given as the dash−dotted line in Figure 2, is predominantly in resonance with the (6,5), (8,1), and (7,3) tubes. Resonant excitation should therefore lead to a similar excitation density N (per unit tube length) in these chiralities, while N in the (7,5) tube is expected to be significantly less because it is clearly off-resonance. After resonant excitation, we can therefore expect a reduction of the (7,5) PB with respect to the other PB features. However, Figure 2 shows that the opposite is observed: the excitation density on the (7,5) tube is clearly higher than in the other chiralities. We conjecture that the *excess exciton density* on the (7,5) tubes with respect to resonant excitation is caused by ET from the resonantly excited tubes, predominantly from the (6,5) tube. The conjecture of ET from the (6,5) to the (7,5) tubes is in line with the observation of a delayed population rise of the (7,5) PB in Figure 3, and with the fact that the excess exciton density on the (7,5) tubes is much higher in sample 2 than in sample 1. From a rough analysis of Figure 3, we conclude that ET from the (6,5) to the (7,5) tubes occurs in less than 20 fs.

To obtain a refined value for the ET rate, we need to consider that the spectral evolutions shown in Figure 3 are not only due to population transfer but also show coherent effects, as can be clearly seen from the spec-

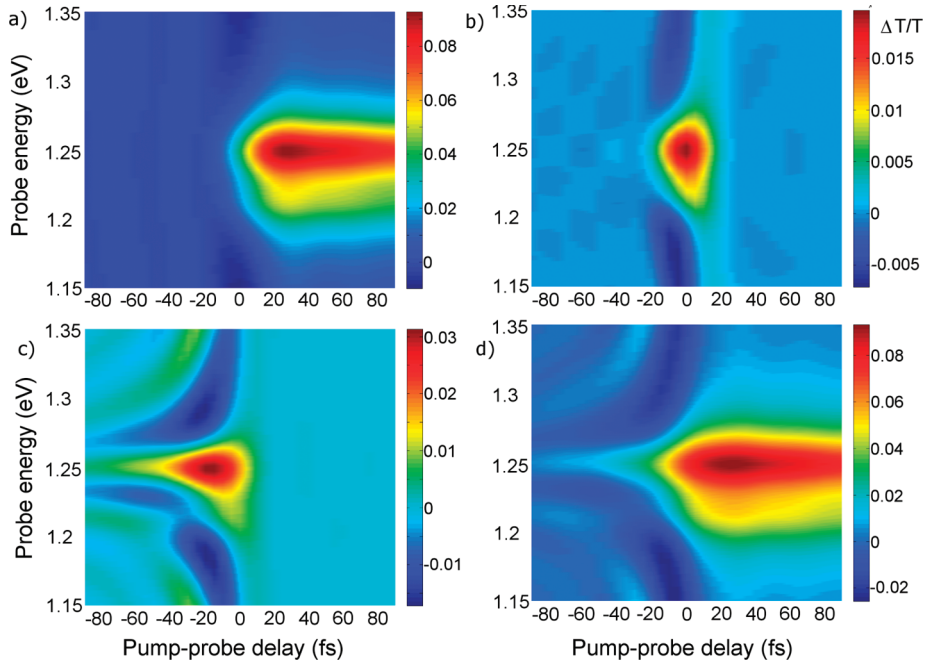

Figure 4. Calculation of coherent contributions to total $\Delta T/T$ spectrum according to ref 24: (a) population, (b) coherent coupling, (c) pump perturbed probe free induction decay, (d) overall signal.

tral oscillations at negative times (minimum $\Delta T/T$ shifts to the blue for $t \rightarrow 0$). To separate coherent effects from population, we are now going to predict the coherent effects, based on our knowledge about the pump/probe pulses and the electronic resonances, which will allow us to subtract the coherent effects from the $\Delta T/T$ spectra, retaining the pure population contribution. We use the approach by Brito Cruz *et al.*[24] This theory is based on the perturbative approach for the third order nonlinear response of the two-level system and describes the pump−probe signal as a superposition of three contributions, worked out separately: polarization coupling, pump-perturbed free induction decay (PPFID), and population dynamics. To account for the actual experiment, we consider two electronic resonances: one represents the $S_0 \rightarrow S_1$ transition of the (7,5) tubes at 1.21 eV, while the other chiralities ((6,5), (7,3), and (8,1)) are represented by a single oscillator at 1.25 eV; this is justified by their spectral proximity leading to their appearance as a single band in the film absorption spectra (compare Figure 1 and dashed lines in Figure 2). In the weakly absorbing regime, the calculation can be done by solving the equations separately for either of the two resonances and then simply summing them up according to their assumed spectral weight. This allows us to quantify the coherent contributions to the overall $\Delta T/T$ spectrum, to subtract them from raw data and obtain the pure population dynamics. We highlight that in the calculation of the coherent effects, energy transfer is *not* taken into account, because a delayed population transfer has negligible influence on the coherent effects that arise from an interaction between the pump field and resonant electronic states for a probe pulse preceding or overlapping with the pump. We demonstrate our approach with sample 1, in which the coherent spectral oscillations at negative times are much clearer than in sample 2. This is probably a consequence of enhanced inhomogeneous broadening in the latter. However, an analogous treatment of sample 2, not shown here, led to a similar result.

In Figure 4 we show the results of our calculations, which predict substantial contributions of polarization coupling (Figure 4b) and PPFID (Figure 4c) that add to the pure population dynamics (Figure 4a) and form the total $\Delta T/T$ spectrum (Figure 4d). Please note that the formalism of ref 24 contains no free parameter that would allow weighting the coherent contributions against the population dynamics. In spite of these restrictions, the calculation reproduces the measured transient absorption spectrum quite well; compare Figure 5a to Figure 4d. To highlight quantitative agreement between calculation and theory, we extract in Figure 5c single time traces at probe energies which are dominated by PPFID (blue curves, $E_{pr} = 1.25$ eV) and by polarization coupling (red curves, $E_{pr} = 1.30$ eV). We find that both temporal behavior and absolute dynamics are rendered very well, showing that we successfully isolated coherent effects from population dynamics. To obtain pure population dynamics from the experiment, we therefore can subtract the contributions of polarization coupling and PPFID from the measured $\Delta T/T$ spectrum in Figure 5a. The result is shown in Figure 5b. The successful removal of coherent effects is evidenced by the absence of the tailing of the PB into the negative time region and the strong reduction of spec-

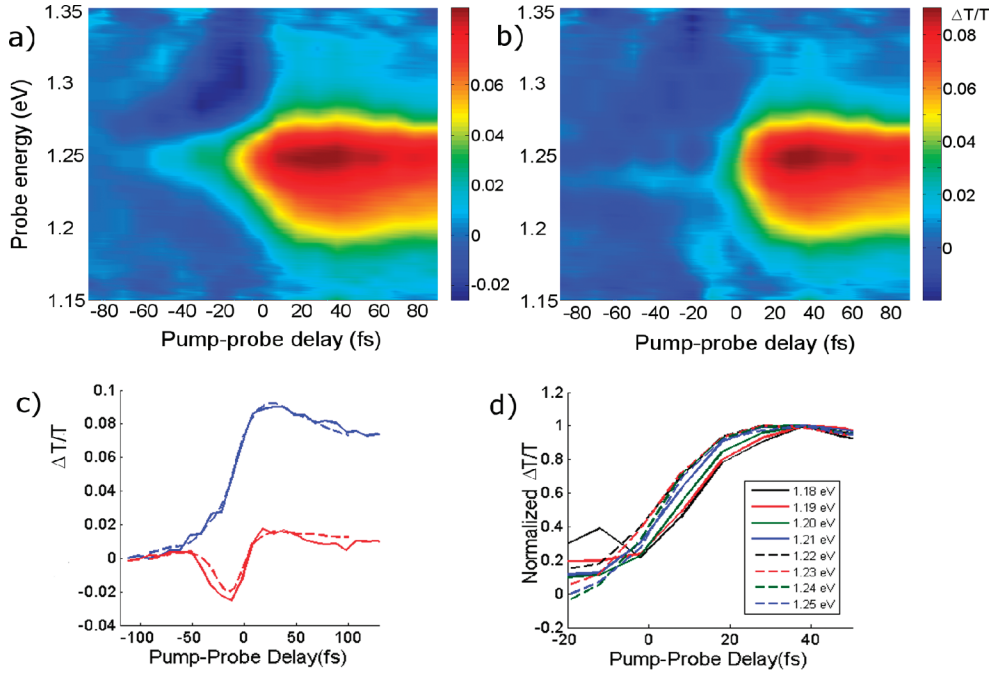

Figure 5. (a) Measured $\Delta T/T$ spectrum in sample 1 as a function of probe energy and delay. (b) Pure population contribution to panel a obtained by subtraction of the coherent contributions (Figure 4 panels b and c) from Figure 5a. (c) Experimental and calculated time traces at fixed probe energy, obtained from horizontal cuts through Figures 5a and 4d, respectively. Solid curves, experimental data; dashed curves, calculated data; blue curves, 1.25 eV; red curves, 1.30 eV. (d) Normalized time traces of population build-up, obtained as horizontal cuts through panel b at various probe energies.

tral oscillations at negative times. In Figure 5d, we report horizontal cuts (single time traces) at various probe energies, representing population rise curves. It becomes evident that at probe energies dominated by the PB of the (7,5) tube, population rise is delayed by about 10 fs against the population rise of the (6,5) tube. This result allows us to fix an upper limit of the energy transfer time of 10 fs.[25] This transfer time is orders of magnitude shorter than the competing relaxation to the electronic ground state of the (6,5) tubes, occurring within picoseconds.[3] Nonetheless, the ET yield is far less than unity, as evidenced by a significant residual (6,5) PB after ET toward (7,5). In sample 1, the residual (6,5) PB can be explained by the dominance of isolated tubes and small aggregates composed of only 2 or 3 CNTs; in such a case, the probability to include in the aggregate an acceptor tube for the (6,5) tube (with an S_1 exciton lower in energy than that of the (6,5) tube) is far below unity, as can be estimated from Figure 1c. However, in sample 2, with up to seven-member aggregates and a higher concentration of low optical bandgap CNTs, statistics predicts the presence of at least one acceptor tube in nearly every aggregate. Still, we observe only partial ET in sample 2. Such a partial ET has recently been explained by efficient phonon-mediated backtransfer from (7,5) to (6,5) because the respective S_1 energies are within kT, making these phonons thermally populated.[15] Our measurements confirm this picture and show that the achievement of the equilibrium between forward and back energy transfer occurs in less than 10 fs. The fact that we do not observe any population dynamics between the (6,5) tube and the (8,1) and (7,3) tubes, is explained on the same footing: energetic proximity of their respective S_1 excitons leads to nearly equal occupation in thermal equilibrium, so the population dynamics after resonant excitation will be negligible. The authors of ref 15 note that apart from energetic considerations, energy transfer might also be inhibited by a strong exciton momentum mismatch, occurring when the dispersion curves of the involved exciton bands differ strongly. In our case, the Brillouin zones for the S_1 excitons of both (6,5) and (7,5) tubes are very similar, so ET in both directions will be favored. On the other hand, the Brillouin zone of the S_1 state of the (8,4) tube differs strongly from that of the (6,5) tube leading to strongly different momenta for S_1 excitons of the same energy. This might explain why the (8,4) tube, which is present in sample 2 in significant concentration, is not an efficient acceptor from either (6,5) or (7,5), as has been demonstrated in a previous study (at 200 fs resolution) showing the absence of excess exciton density on the (8,4) tube.[26]

If the ET time is shorter than the relaxation time from S_2 into S_1 (the latter estimated around 40 fs)[27] the observation of ET within the second excitonic manifold is possible. In Figure 6, we present time-resolved $\Delta T/T$ spectra in the region of the S_2 resonance for both samples. In these experiments both pump and probe are 7 fs visible pulses, so here the instrumental resolution of about 10 fs is higher than for the experiments discussed above. Sample 1 shows a rather simple behavior: at time zero, we see PB features around 1.8 and

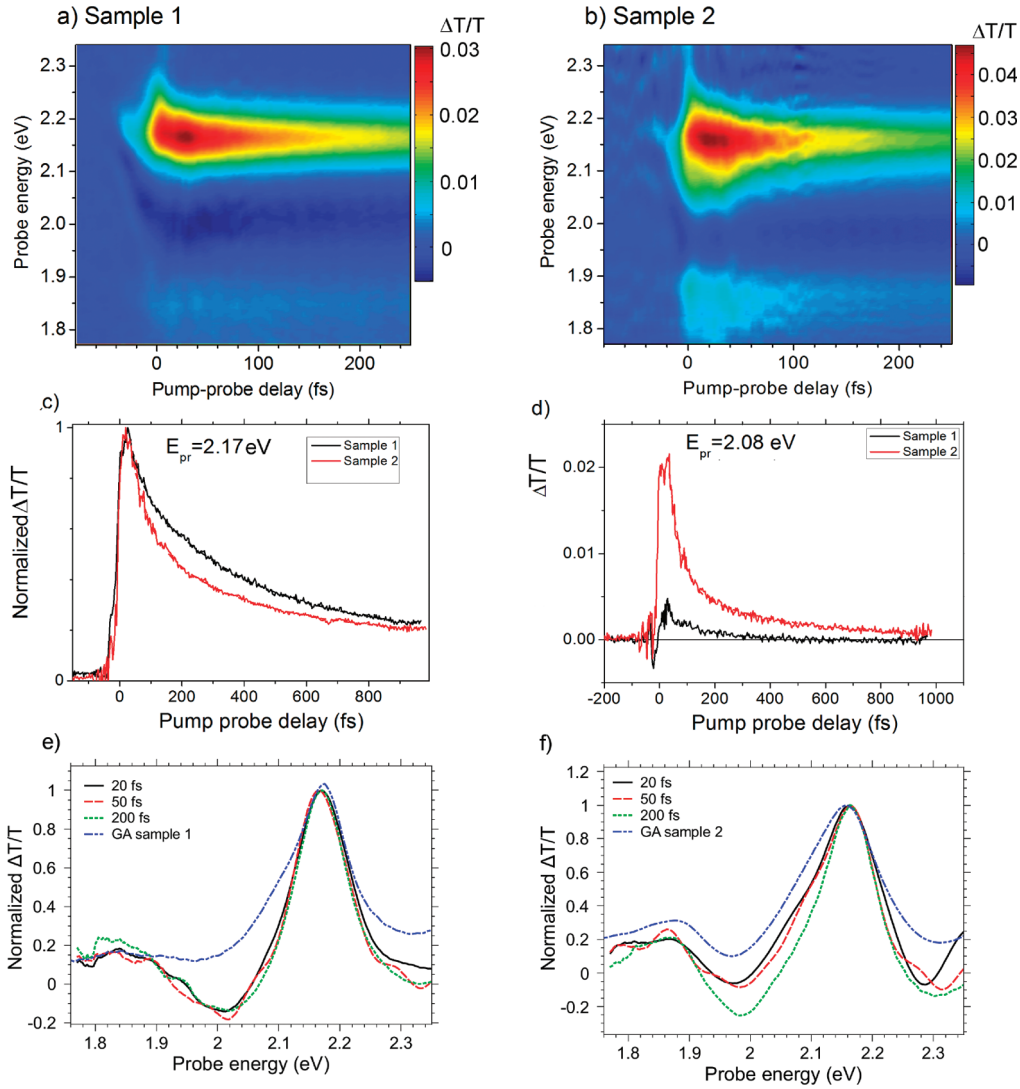

Figure 6. (a and b) Δ*T*/*T* spectra of samples 1 and 2, respectively, using 7 fs degenerate broadband pulses for pump and probe. Coherent oscillations of the G mode frequency can clearly be seen and are a sign of high time resolution; their phase profile shows that the pulses are nearly transform-limited (chirp-free). (c and d) Time traces (full curves) at 2.17 and 2.08 eV, respectively, and biexponential fits (dashed lines). The fitting parameters are given in Table 1. (e and f) Single normalized pump probe spectra (vertical sections through panels a and b, respectively) for sample 1 and 2, respectively. For comparison, the ground state absorption (GA) spectra are given as dash-dotted lines

2.15 eV and a PA band at 2.0 eV. All of these features decay on a several hundred femtosecond time-scale. During decay, there is negligible spectral evolution, as can be clearly seen in Figure 6e. A biexponential fit reproduces the time trace at 2.17 eV (Figure 6c). The fast process with 39 fs decay constant accounts for 37% of the total dynamics and is caused by internal conversion from the S_2 to the S_1 manifold[27] Even when all of the population has decayed into the S_1 manifold of the tubes, S_2 still remains partially bleached; this is most likely due to the common ground state of the excitonic transitions. The absence of spectral evolution during decay in sample 1 is an important point because it highlights that the dynamics, obtained from the biexponential fit, are valid not only for the dominant (6,5) tubes, but also for the other tubes that have been resonantly excited. In particular, we conclude that the (6,4) and (8,4) tubes, with their S_2 resonances slightly red-shifted with respect to that of the (6,5) tube (see Figure 1c), relax to the S_1 manifold with 40 fs time constant but still retain a partial bleach of the S_2 due to the presence of a common ground state. The absence of spectral evolution in sample 1 thus allows us to conclude that on the time scale of the experiment, the *excitation density N* of the S_1 states remains similar for the (6,5) and the minority tubes.

TABLE 1. Biexponential Fit Parameters From Figure 6, Panels c and d

sample	E_{pr} (eV)	τ_1 (fs)	A_1 (% of total dynamics)	τ_2 (fs)	A_2 (% of total dynamics)
1	2.17	39	37	368	63
2	2.17	52	59	336	41
2	2.08	42	82	400	18

Sample 2, when compared to sample 1, shows quite different dynamics and spectral shape: The initial PB feature around 2.15 eV is clearly broadened with respect to sample 1. Since the GA spectrum of sample 2 is broadened as well compared to that of sample 1, we can ascribe the initial PB broadening in sample 2 to enhanced resonant excitation of chiralities whose S_2 resonance is slightly red-shifted with respect to the one of the (6,5) tube. During decay, spectral narrowing occurs on a time scale of 100 fs. Single spectra at 20, 50, and 200 fs time delay in Figure 6f show the presence of a shoulder at 2.08 eV at very early times, which decays much faster than the main PB peak at 2.15 eV. Referring to the common ground state for S_1 and S_2 states, valid for all excited chiralities, we can explain this narrowing by a strongly accelerated population loss of both S_2 and S_1 for one or both of the minority CNTs (6,4) or (8,4). Since the narrowing occurs only in sample 2, containing a high percentage of aggregates, we ascribe the population loss to an intertube transfer event. In sample 2, the concentration of (8,4) is much higher than that of (6,4), so that we ascribe the population loss predominantly to the (8,4) tube. Addressing the question whether an exciton or a single charge is transferred, we note that in the latter case, the PB of the originally occupied tube would remain, due to the presence of the countercharge. The observation of strong population loss is therefore an indication for ET rather than charge transfer.

Comparing time traces, we see that at 2.17 eV (Figure 6c) sample 2 has a much stronger contribution of the initial fast decay, (59% against 37%), with a time constant of 52 fs. At 2.08 eV (Figure 6d), the decay dynamics is entirely dominated by the fast decay process, with only a weak contribution of the slower one. We find 42 fs lifetime for the fast process with a relative weight of 82%.

To quantify the dynamics of this spectral narrowing, that only occurs in sample 2, we compared the biexponential fits at selected probe wavelengths in samples 1 and 2.[28] The obtained fast and slow decay times, as well as their relative contribution to the overall decay dynamics, are given in Table 1. Please note that due to the absence of spectral evolution in sample 1, the observed dynamics at 2.17 eV is representative for the whole spectral region while in sample 2, a strong dependence on the probe energy becomes evident. The slow decay time is not systematically sample dependent; it is related to dispersive nonradiative decay of S_1 to the ground state.[20] The fast decay time is slower in sample 2 than in sample 1. The largest difference is however seen in the relative weights of the processes. The fast process is much more dominant in sample 2 than in sample 1. At 2.08 eV, it accounts for 82% of the total decay, while in sample 1, its contribution is only 37%. The probe energy 2.08 eV is close to the S_2 resonance of both the (6,4) and (8,4) tubes; indeed Figure 6f evidence a shoulder at this spectral position. Therefore this observation is consistent with fast population loss of the (6,4) and (8,4) tube due to energy transfer. However, we need to assess whether the population is transferred from the S_2 or the S_1 state. If it were transferred from S_2, then internal conversion toward S_1 and energy transfer would compete, adding up to an increased overall decay rate. In the absence of any process competing with internal conversion, the relative weight A_2 is supposed to be 50% because the contribution of stimulated emission (occurring only in S_2) to the observed positive band should equal the amount of pure PB from the common ground state (occurring in both S_2 and S_1). Experimentally, at 2.08 eV we find $A_2 = 18\%$, so the yield of S_1 production is only $18/50 = 0.36$. Consequently, the ET yield defined as $\Phi_{ET} = \tau_{tot}/\tau_{ET}$ with the overall decay time $1/\tau_{tot} = 1/\tau_{ET} + 1/\tau_{21}$, where τ_{21} is the internal conversion time, should be at least 64%. If there is spectral overlap with other chiralities at 2.08 eV, then $\Phi_{ET} > 0.64$. Since at 2.08 eV in sample 2, $\tau_{tot} = 42$ fs, we obtain $\tau_{ET} < 65.6$ fs and $\tau_{21} > 117$ fs. The internal conversion time, postulated here, is in stark contrast with the measured one on the isolated CNTs (see Figure 6a), which holds for all chiralities including the (8,4). Therefore, we discard this scenario and conclude that ET from (8,4) takes place after S_2-S_1 internal conversion. In this case, the overall decay time is expected to increase with respect to pure internal conversion, which indeed is observed experimentally (42 against 39 fs at 2.08 eV for sample 2 and 1, respectively). From the difference in the experimental decay between sample 1 and 2, we conclude that the ET time should be below 10 fs. We note that we do not expect to see a clear population build-up anywhere in the spectrum, since the rate-limiting step for ET is internal conversion. As a consequence, the population transfer toward other chiralities occurs on the same time scale as their "own" internal conversion, leading only to a slight apparent slowing down of the latter.

Considering the S_1 energies of the chiralities (Figure 1c), we find that in sample 2, the (8,4) tubes, although being relatively low-energy tubes, still find sufficient neighbors with even lower S_1 energy. As we have noted above, the transfer from (6,5) toward (8,4), that should be energetically favored in S_1 and lead to a depopulation of (6,5), is not observed even in sample 2 probably due to a momentum mismatch between the respective S_1 excitons.

There are alternative scenarios leading to a short-lived spectral broadening, as shown here, among which are biexcitons[29] or two-photon excitations.[7] However, the absence of this short-lived broadening in sample 1 clearly argues against such kinds of states, because their formation does not require intertube interaction. Moreover, also the coincidence of the spectral position of the short-lived shoulder in Figure 6f with the S_2 reso-

nance of the (8,4) tube speaks against an effect occurring in (6,5) tubes.

CONCLUSIONS

We have reported direct evidence for ultrafast energy transfer between aggregated tubes of different chirality. We have found ET from the (6,5) to the (7,5) tube as well as from the (8,4) and (6,4) tubes to a manifold of acceptor tubes. In both cases, the transfer occurred in the S_1 state although in the second case the S_2 state was populated resonantly. In both cases we found that the transfer is not instantaneous, and determined an upper limit for the transfer time of 10 fs. This exceptionally short transfer time poses the question of the possible transfer mechanism. We can rule out Foerster type dipole−dipole coupling, because this approximation breaks down at the high transfer rates that we find.[30] One possibility is the full Coulomb multipolar coupling, involving also "dark" (nondipole allowed) and coherent states, followed by ultrafast relaxation, characterizing the "intermediate coupling regime" of resonance energy transfer. Additionally, tunneling[31] and superexchange, or Dexter transfer *via* wave function overlap might play a role. The latter could take place because of the cylindrical symmetry and the pseudohexagonal lattice in the bundles which suggest strong $\pi-\pi$ interaction. At this stage, we cannot be more specific in our assignment and leave the question open for further theoretical investigations.

ET studies after pumping resonantly the S_2 excitons did not show any clear evidence for ET from S_2. This result is mainly based on the absence of a clear ultrafast population transfer from (6,5) toward (8,4) in sample 2. This couple is however affected by momentum mismatch of the respective excitons, strongly suppressing ET; therefore this result should not be generalized.

So far, ET has been largely ignored in the development of a theory for the electronic structure and dynamics of CNT networks. Near future applications however will indeed regard such networks more than single tubes, and the phenomena here investigated will be determinant for understanding and improving device performances.

METHODS

Single-wall carbon nanotubes (SWeNT SG 65) were enriched by diameter using density gradient ultracentrifugation, and solid films were prepared by incorporating the supernatant in a xerogel gelatin matrix; details of the procedure can be found elsewhere.[3] We compared samples with different degrees of aggregation: sample 1 consisted predominantly of isolated (6,5) tubes and very small aggregates (2 or 3 tubes in a pseudohexagonal lattice) enriched by density gradient ultracentrifugation, and sample 2 consisted predominantly of small tube aggregates (up to 7 tubes) commonly what is found in traditional nanotube colloidal suspensions.[32] Hence, effects that are induced by intertube interaction should be strongly enhanced in sample 2.

Near infrared light pulses in the 900−1100 nm wavelength region were generated by a home-built noncollinear optical parametric amplifier (NOPA)[33] and compressed to nearly transform-limited 15-fs duration by a fused silica prism pair. Visible pulses in the wavelength region of 500−700 nm were obtained by a similar NOPA, operated under a different angle to allow broadband phase matching. The resulting pulses were compressed close to the Fourier transform limit by a pair of doubly chirped mirrors, resulting in virtually chirp free pulses of about 7 fs duration.[33] We used a degenerate pump−probe setup equipped with fast spectral acquisition *via* a computer-controlled optical multichannel analyzer (OMA) enabling single-shot detection at the full 1 kHz repetition rate. This setup allows recording two-dimensional (2D) differential transmission ($\Delta T/T$) maps as a function of probe wavelength and delay in a few minutes measurement time with high sensitivity. Pump and probe pulses pass through the same focusing mirrors and thus have an equal spot size of about 60 μm, as measured by the "razor blade method". Instrumental response function and time zero were verified daily by measuring the cross-correlation of the pump and probe pulses. More details of the experimental setup have been published elsewhere.[34] CNT graphics were built using QuteMol.[35]

Acknowledgment. This work was financially supported by the European Commission through the Human Potential Programme (Marie-Curie RTN BIMORE, Grant No. MRTN-CT-2006-035859).

REFERENCES AND NOTES

1. Avouris, P.; Chen, J. Nanotube Electronics and Optoelectronics. *Mater. Today* **2006**, *9*, 46–54.
2. Ando, T. Excitons in Carbon Nanotubes. *J. Phys. Soc. Jpn.* **1997**, *66*, 1066–1073.
3. Lüer, L.; Hoseinkhani, S.; Polli, D.; Crochet, J.; Hertel, T.; Lanzani, G. Size and Mobility of Excitons in (6, 5) Carbon Nanotubes. *Nat. Phys.* **2009**, *5*, 54–58.
4. Qiu, X.; Freitag, M.; Perebeinos, V.; Avouris, P. Photoconductivity Spectra of Single-Carbon Nanotubes: Implications on the Nature of Their Excited States. *Nano Lett.* **2005**, *5*, 749–752.
5. Chen, J.; Perebeinos, V.; Freitag, M.; Tsang, J.; Fu, Q.; Liu, J.; Avouris, P. Bright Infrared Emission from Electrically Induced Excitons in Carbon Nanotubes. *Science* **2007**, *310*, 1171–1174.
6. Beard, M. C.; Blackburn, J. L.; Heben, M. J. Photogenerated Free Carrier Dynamics in Metal and Semiconductor Single-Walled Carbon Nanotube Films. *Nano Lett.* **2008**, *8*, 4238–4242.
7. Wang, F.; Dukovic, G.; Brus, L. E.; Heinz, T. F. The Optical Resonances in Carbon Nanotubes Arise from Excitons. *Science* **2005**, *308*, 838–841.
8. Cao, Q.; Kim, H.-S.; Pimparkar, N.; Kulkarni, J. P.; Wang, C. J.; Shim, M.; Roy, K.; Alam, M. A.; Rogers, J. A. Medium-Scale Carbon Nanotube Thin-Film Integrated Circuits on Flexible Plastic Substrates. *Nature* **2008**, *454*, 495–502.
9. Crochet, J.; Clemens, M.; Hertel, T. Optical Properties of Structurally Sorted Single-Wall Carbon Nanotube Ensembles. *Phys. Stat. Sol. B* **2007**, *244*, 3964–3968.
10. Kato, T.; Hatakeyama, R. Exciton Energy Transfer-Assisted Photoluminescence Brightening from Freestanding Single-Walled Carbon Nanotube Bundles. *J. Am. Chem. Soc.* **2008**, *130*, 8101–8107.
11. Tan, P. H.; Rozhin, A. G.; Hasan, T.; Hu, P.; Scardaci, V.; Milne, W. I.; Ferrari, A. C. Photoluminescence Spectroscopy of Carbon Nanotube Bundles: Evidence for Exciton Energy Transfer. *Phys. Rev. Lett.* **2007**, *99*, 137402.
12. Torrens, O. N.; Milkie, D. E.; Zheng, M.; Kikkawa, J. M. Photoluminescence from Intertube Carrier Migration in Single-Walled Carbon Nanotube Bundles. *Nano Lett.* **2006**, *6*, 2864–2867.

13. Chen, F.; Ye, J.; Teo, M. Y.; Zhao, Y.; Tan, L. P.; Chen, Y.; Chan-Park, M. B.; Li, L. J. Species-Dependent Energy Transfer of Surfactant-Dispersed Semiconducting Single-Walled Carbon Nanotubes. *J. Phys. Chem. C* **2009**, *113*, 20061–20065.
14. Harutyunyan, H.; Gokus, T.; Green, A. A.; Hersam, M. C.; Allegrini, M.; Hartschuh, A. Photoluminescence From Disorder Induced States in Individual Single-Walled Carbon Nanotubes. *Phys. Stat. Sol. B* **2009**, *246*, 2679–2682.
15. Lefebvre, J.; Finnie, P. Photoluminescence and Förster Resonance Energy Transfer in Elemental Bundles of Single-Walled Carbon Nanotubes. *J. Phys. Chem. C* **2009**, *113*, 7536–7540.
16. Qian, H.; Georgi, C.; Anderson, N.; Green, A. A.; Hersam, M. C.; Novotny, L.; Hartschuh, A. Exciton Energy Transfer in Pairs of Single-Walled Carbon Nanotubes. *Nano Lett.* **2008**, *8*, 1363–1367.
17. Absorption spectra in suspension are sharper than in solid matrix, therefore we use suspension spectra for the determination of the chirality distribution. Note that matrix formation is neutral to the chirality distribution.
18. S_1 (S_2) is the excitonic states that is created by a one-photon allowed transition between the lowest (second lowest) valence and conduction bands E11 (E22).
19. Ju, S.-Y.; Kopcha, W. P.; Papadimitrakopoulos, F. Brightly Fluorescent Single-Walled Carbon Nanotubes *via* an Oxygen-Excluding Surfactant Organization. *Science* **2009**, *323*, 1319–1323.
20. Zhu, Z. P.; Crochet, J.; Arnold, M. S.; Hersam, M. C.; Ulbricht, H.; Resasco, D.; Hertel, T. J. Pump−Probe Spectroscopy of Exciton Dynamics in (6,5) Carbon Nanotubes. *Phys. Chem. C* **2007**, *111*, 3831–3835.
21. Note that for $t < 10$ fs, PA at energies >1.25 eV does occur. This is however a coherent effect, as evidenced by the dynamic shift of the band minimum. In the following section, we are going to separate coherence from population.
22. Sau, J. D.; Cohen, M. L. Possible Electric-Field-Induced One-Dimensional Excitonic Insulators in Pairs of Carbon Nanotubes. *Phys. Rev. B* **2008**, *78*, 115436.
23. Kim, K. K.; Bae, J. J.; Park, H. K.; Kim, S. M.; Geng, H.-Z.; Park, K. A.; Shin, H.-J.; Yoon, S.-M; Benayad, A.; Choi, J.-Y; *et al*. Fermi Level Engineering of Single-Walled Carbon Nanotubes by $AuCl_3$ Doping. *J. Am. Chem. Soc.* **2008**, *130*, 12757–12761.
24. Brito Cruz, C. H.; Gordon, J. P.; Becker, P. C.; Fork, R. L.; Shank, C. V. Dynamics of Spectral Hole Burning. *IEEE J. Quantum Electron.* **1988**, *24*, 261–266.
25. Note that in this experiment, a small residual "chirp" of the pump and probe pulses on the order of a few femtoseconds is possible, so that we can only give an upper limit of the transfer time.
26. Lüer, L.; Lanzani, G.; Crochet, J.; Hertel, T.; Holt, J.; Vardeny, Z. V. Ultrafast Dynamics in Metallic and Semiconducting Carbon Nanotubes. *Phys. Rev. B* **2009**, *80*, 205411.
27. Manzoni, C.; Gambetta, A.; Menna, E.; Meneghetti, M.; Lanzani, G.; Cerullo, G. Intersubband Exciton Relaxation Dynamics in Single-Walled Carbon Nanotubes. *Phys. Rev. Lett.* **2005**, *94*, 207401.
28. We did not separate coherent contributions in Figure 6 because these are expected to occur on a sub-10 fs time scale when 7 fs pump and probe pulses are deployed, while the dynamics of interest occur on a 50 fs time scale.
29. Pedersen, T. G.; Pedersen, K.; Cornean, H. D.; Duclos, P. Stability and Signatures of Biexcitons in Carbon Nanotubes. *Nano Lett.* **2005**, *5*, 291–294.
30. Scholes, G. D. Long-Range Resonance Energy Transfer in Molecular Systems. *Annu. Rev. Phys. Chem.* **2003**, *54*, 57–87.
31. Li, H.; Loke, W. K.; Zhang, Q.; Yoon, S. F. Physical Device Modeling of Carbon Nanotube/GaAs Photovoltaic Cells. *Appl. Phys. Lett.* **2010**, *96*, 043501.
32. Crochet, J.; Clemens, M.; Hertel, T. Quantum Yield Heterogeneities of Aqueous Single-Wall Carbon Nanotube Suspensions. *J. Am. Chem. Soc.* **2007**, *129*, 8058–8059.
33. Manzoni, C.; Polli, D.; Cerullo, G. Two-Color Pump−Probe System Broadly Tunable over the Visible and the near Infrared with Sub-30 fs Temporal Resolution. *Rev. Sci. Instrum.* **2006**, *77*, 023103.
34. Polli, D; Lüer, L.; Cerullo, G. High-Time-Resolution Pump−Probe System with Broadband Detection for the Study of Time-Domain Vibrational Dynamics. *Rev. Sci. Instrum.* **2007**, *78*, 103108.
35. Tarini, M.; Cignoni, P.; Montani, C. Ambient Occlusion and Edge Cueing for Enhancing Real Time Molecular Visualization. *IEEE Trans. Visualization Comput. Graph.* **2006**, *12*, 1237–1244.
36. Bachilo, S. M.; Strano, M. S.; Kittrell, C.; Hauge, R. H.; Smalley, R. E.; Weisman, R. B. Structure-Assigned Optical Spectra of Single-Walled Carbon Nanotubes. *Science* **2002**, *298*, 2361–2366.